I&EC research
Industrial & Engineering Chemistry Research

Article

pubs.acs.org/IECR

Photocatalytic Reduction of CO_2 Using Ti−MCM-41 Photocatalysts in Monoethanolamine Solution for Methane Production

Hung-Yu Wu,[†] Hsunling Bai,*[,†] and Jeffrey C. S. Wu[‡]

[†]Institute of Environmental Engineering, National Chiao Tung University, Hsinchu, 30010, Taiwan

[‡]Department of Chemical Engineering, National Taiwan University, Taipei, 10617, Taiwan

ABSTRACT: Photocatalytic reduction of carbon dioxide (CO_2) to form a valuable energy source of methane (CH_4) in monoethanolamine (MEA) solution is first investigated by mesoporous photocatalysts of Ti−MCM-41 in this study. The MEA solution was chosen as the absorbent and reductant because amine absorption is one of the most popular methods for CO_2 capture from flue gas streams. Also, it is intended to integrate the CO_2 capture and utilization into one process. The photocatalytic results of methane yields indicated that MEA served as a better reductant than water and NaOH which have been commonly used for CO_2 reduction. For the best photocatalyst of Ti−MCM-41(50) manufactured at a Si/Ti molar ratio of 50, its methane yield (62.42 μmol/g of cat.) was much higher than that of commercial P25 photocatalyst after 8 h of UV illumination. A photoreduction quantum efficiency (PQE) of 9.18% was achieved.

1. INTRODUCTION

The global warming issue is one of the major environmental concerns due to the rising demand for energy which leads to a significant increase in CO_2 greenhouse gas emissions.[1,2] At present, CO_2 capture and storage (CCS) has been evaluated by the Intergovernmental Panel on Climate Change (IPCC) as a feasible CO_2 mitigation option.[3] The monoethanolamine (MEA) absorption process has been demonstrated to be one of the most mature CO_2 capture processes from flue gases of fossil fuel fired power plants and other large industrial processes.[4,5] The CO_2 could be stripped from the MEA−CO_2 absorption/stripping process at the cost of an energy penalty. Besides, due to the environmental concerns of CO_2 storage in the deep sea or underground, it is usually difficult to find appropriate storage sites. Thus, it is viable to reutilize the absorbed CO_2.

The current CO_2 reutilization techniques include various biotechnologies[6,7] or chemical processes[8−10] to produce valuable chemicals or new energy, which may provide another option rather than the storage of CO_2. However, to the authors' knowledge, although there have been literature studies on using water, NaOH, and 2-propanol as the reducing agents of CO_2 photocatalytic reduction,[10−13] there is no literature reporting on using MEA as the photocatalytic reducing agent of CO_2.

One of the key factors for enhancing photocatalytic activity is to increase the surface area of the photocatalyst.[14] Therefore, porous materials such as silica, activated carbon, and zeolite were employed with photocatalysts.[15−17] The incipient wetness technique and the ion-exchange method have been used to attain high surface areas of photocatalysts, where the porous material was impregnated with metal precursors in the solution phase and followed by activation under a reducing atmosphere.[18−20]

Since it might be economical if the CO_2 capture technology is combined with the CO_2 photocatalytic reduction process and produce a valuable energy source such as methane (CH_4), this study intends to evaluate the possibility of using the CO_2 absorption reagent of MEA as the photocatalytic reducing agent of CO_2. The obtained Ti−MCM-41 photocatalysts were characterized by X-ray diffraction (XRD), Brunauer−Emmett−Teller (BET), transmission electron microscopy (TEM), Fourier transform infrared spectroscopyt (FT-IR), and X-ray photoelectron spectroscopy (XPS) analyses. The performance of the photocatalytic reduction of CO_2 in MEA, NaOH, and water solutions was compared in terms of the CH_4 production rate. The effect of the Si/Ti molar ratio in the Ti−MCM-41 photocatalytic materials on the CH_4 yield was evaluated, and the photoreduction quantum efficiency was reported.

2. MATERIALS AND METHODS

2.1. Catalyst Preparation. Ti−MCM-41 mesoporous photocatalysts with Si/Ti molar ratios of 200, 100, and 50 were synthesized by a hydrothermal method using sodium metasilicate ($Na_2SiO_3{\cdot}9H_2O$) and titanium oxysulfate ($TiOSO_4$) as the starting materials. In a typical procedure, 21.2 g of sodium metasilicate was first dissolved in 100 mL of deionized (DI) water.[21,22] Titanium oxysulfate was dissolved in 20 mL of 2 M sulfuric acid (H_2SO_4) and then added dropwise into the above solution. The pH value of the solution was then adjusted to 10.5 using 2 M sulfuric acid followed by further stirring to form a gel. Meanwhile, 7.28 g of cetyltrimethylammonium bromide (CTAB) was dissolved in 25 mL of DI water and then it was added dropwise into the above solution. The molar composition of the solution mixture was SiO_2:*X*Ti:0.2CTAB:0.89H_2SO_4:120H_2O (*X* was the amount of Ti added to obtain different Si/Ti molar ratios). The resulting solution mixture was put in an autoclave and then placed in an oven at 145 °C for 36 h. The resultant solid was

Received: November 5, 2013
Revised: June 17, 2014
Accepted: June 24, 2014
Published: June 24, 2014

dx.doi.org/10.1021/ie403742j | *Ind. Eng. Chem. Res.* 2014, 53, 11221−11227

then recovered by filtration, washed with DI water, and dried in an oven at 120 °C. Finally, the organic template was removed in the oven at 550 °C for 6 h. The photocatalyst was denoted as Ti−MCM-41(Z), where Z (=1/X) was the molar ratio of Si/Ti.

2.2. Catalyst Characterization. Powder low angle X-ray diffraction patterns of calcined mesoporous adsorbents were recorded by an X-ray (wavelength λ = 1.5405 Å) diffractometer (Bruker D8 SSS) equipped with a copper target operated at 30 kV and 20 mA. The diffractograms of the mesoporous samples were recorded in the 2θ range of 2−50° with a scanning speed of 1 deg/min. The morphology of the materials was observed via TEM (JEOL JEM-3000F) images. The photocatalyst samples were mixed and ground with KBr (10:90) and pressed into slices. Then the samples were measured with Fourier transform infrared spectroscopy (FT-IR) (Bruker, Vector 22). The range of the scan was from 400 to 4000 cm^{-1}. X-ray photoelectron spectroscopy (XPS) was used to identify the surface composition of photocatalysts with an ESCA PHI 1600. The metal contents were determined by inductively coupled plasma atomic emission spectroscopy (ICP-AES) using a Jarrell-Ash ICAP9000 instrument. UV−vis diffuse reflectance spectra of samples were measured by using a UV−vis spectrophotometer (HITACHI U3012) equipped with an integral sphere using aluminum oxide (Al_2O_3) as a reference. The spectra of samples were recorded within the range 200−800 nm. The specific surface area, pore volume, and average pore diameter (BJH method) of the samples were measured by N_2 adsorption−desorption isotherms using a surface area analyzer (Micromeritics, ASAP 2000). All the samples were degassed at 350 °C for 6 h under vacuum (10^{-6} mbar) prior to the adsorption experiments.

2.3. Photocatalytic Reduction of CO_2. The experimental setup for the photocatalytic reduction of CO_2 is shown in Figure 1. In the liquid phase reaction, the catalyst loading was

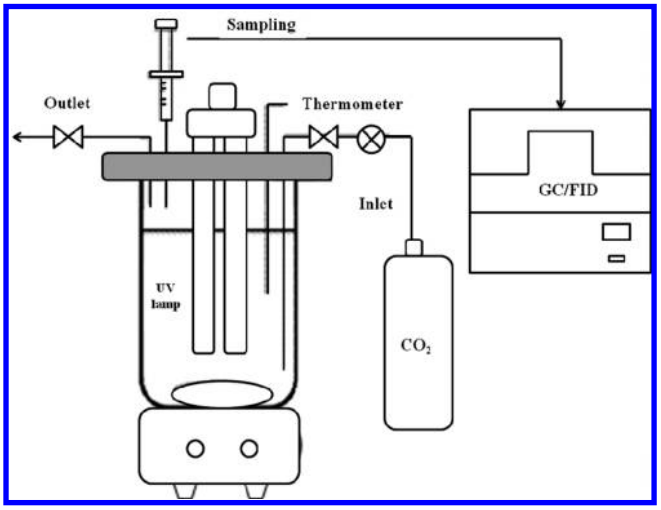

Figure 1. Schematic of experimental setup for photocatalytic reduction of CO_2 using 9 W, 254 nm UV lamp.

0.1 g in 300 mL of solution of reducing agent. MEA, NaOH, and H_2O were respectively used as reducing agents, with solution concentration of 0.2 M for MEA and NaOH. Before each reaction test, the solution was aerated with CO_2 (99.999%) for 1 h to ensure full dissolution of CO_2 in the reducing agents. The experiments were then carried out in a batch reactor with the temperature controlled at 40 °C and Ti−MCM-41 photocatalyst was illuminated in the solution under 9 W and 254 nm of a UVC lamp. The lamp intensity was measured to be 32 $\mu W/cm^2$. The products were analyzed by a gas chromatograph (SRI-8610C) equipped with a flame ionization detector (FID) and 5 m long Porapak Q column. The major product of the reaction was analyzed to be methane.

3. RESULTS AND DISCUSSION

3.1. Catalyst Characterization. Powder X-ray diffraction patterns are shown in Figure 2. It shows that MCM-41 had the

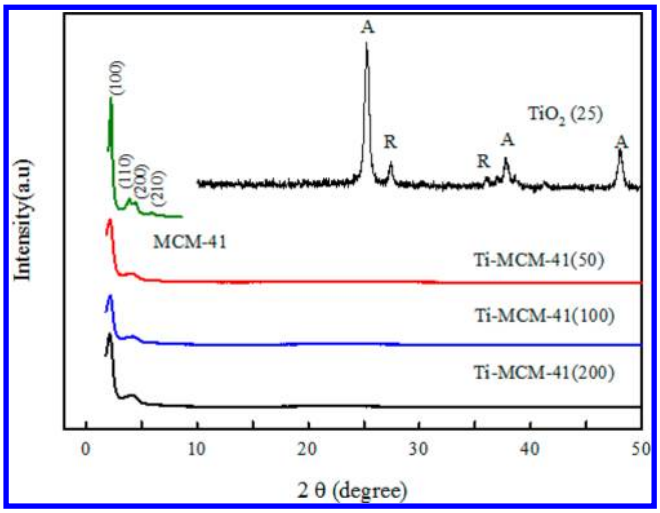

Figure 2. Low angle XRD patterns of MCM-41, Ti−MCM-41, and TiO_2.

regularity of hexagonal columnar structure, which contained four well-defined diffraction peaks of (100), (110), (200), and (210) located at 2θ of 2−10°.[23,24] However, for the Ti−MCM-41 photocatalysts, the low angle XRD patterns exhibited diffraction peaks assigned to (100) and (110) crystal faces only; the intensity of the other two characteristic peaks at (200) and (210) was not very clear. This indicates that the regularity of pore structure was decreased. Nevertheless, the catalysts still retained the mesoporous structure of MCM-41.[25,26] The two diffraction peaks at (100) and (110) were decreased when the amount of Ti content was increased, which revealed that more Ti content doped into the framework of MCM-41 could cause damage to the pore structure. However, the XRD results did not reveal any evidence of TiO_2, which should have peaks appearing from 25 to 43.3°. Thus, the presence of TiO_2 particles on the surface of the MCM-41 mesoporous materials might only be in a minor amount: most of the Ti atoms should be either incorporated into the MCM-41 framework or well dispersed as tiny TiO_2 particles in a small amount.

The pore characteristics and metal contents of mesoporous MCM-41 and Ti−MCM-41 were obtained, and the results are shown in Table 1. The specific surface areas of Ti−MCM-41materials were approximately around 840−850 $m^2\ g^{-1}$ when Si/Ti molar ratios of Ti−MCM-41 were between 200 and 50. It appears that the metal content of Ti in the test range did not significantly affect the specific surface area.

The mesostructure was further confirmed by TEM analysis with results shown in Figure 3 for pure MCM-41 and Ti−MCM-41(50). The TEM image of pure MCM-41 (Figure 3A) clearly shows uniform pore structure and the regularity of hexagonal columnar structure, while the photocatalyst which

Table 1. Pore Characteristics and Metal Contents of Mesoporous Photocatalysts

catalyst	S_{BET} [a] ($m^2\ g^{-1}$)	V_p [b] ($cm^3\ g^{-1}$)	d_{BJH} [c] (nm)	Ti (wt %)	Si/Ti
MCM-41	1065	1.1	3.1		
Ti−MCM-41(200)	853	1.7	2.8	0.21	190
Ti−MCM-41(100)	851	1.4	2.8	0.43	92
Ti−MCM-41(50)	843	2.1	2.8	0.80	50

[a]BET surface area. [b]Pore volume. [c]Pore diameter calculated by BJH theory.

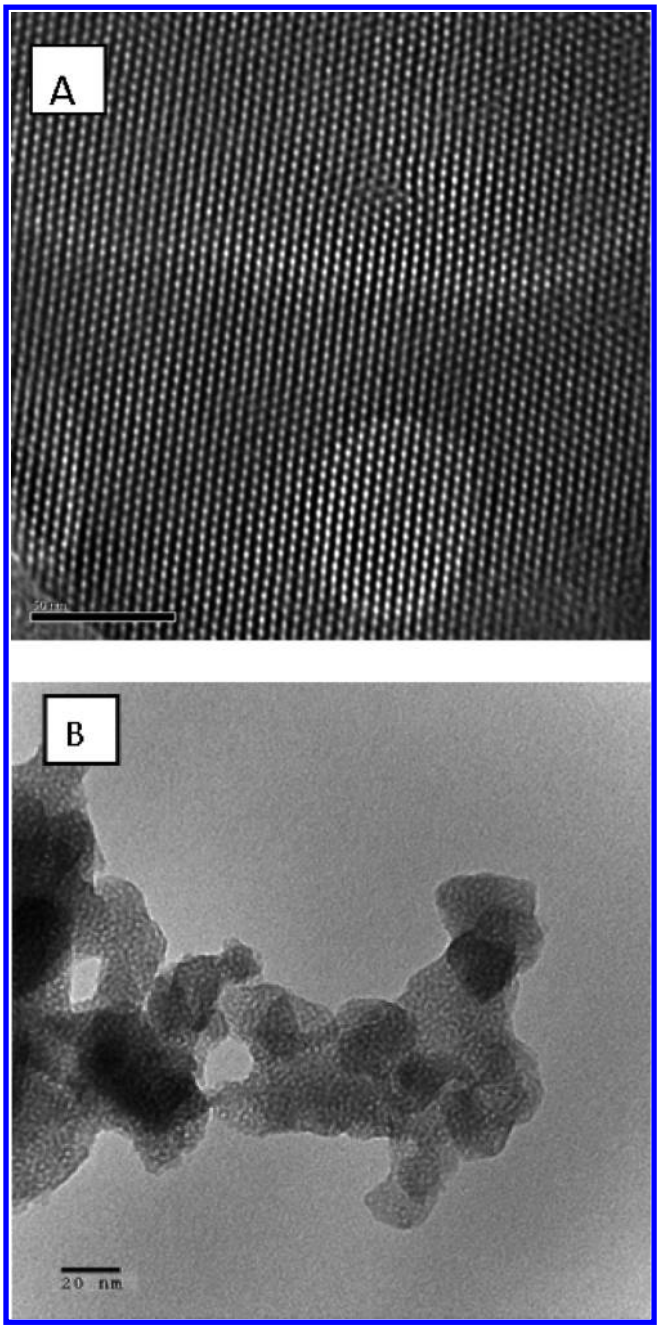

Figure 3. TEM images of (A) pure MCM-41 and (B) Ti−MCM-41(50).

incorporated Ti into MCM-41 showed less regularity of pore structure. Nonetheless, the Ti−MCM-41 photocatalysts still retained a mesoporous structure.

The FT-IR spectroscopic results for MCM-41 and all Ti−MCM-41 materials are shown in Figure 4. The MCM-41

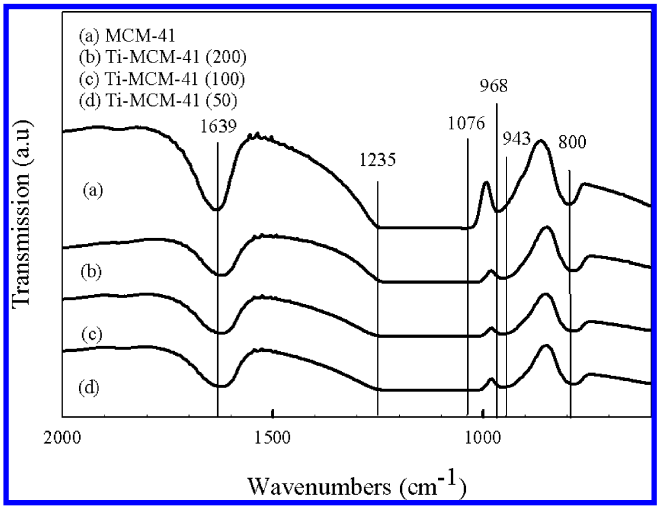

Figure 4. FT-IR spectroscopy result of Ti−MCM-41.

material exhibited Si−O−Si vibration bands[27−29] at 800 cm^{-1}. There should also be peaks at 1076 and 1235 cm^{-1} for the Si−O−Si vibration bands but they are flat lines as observed in Figure 4; this indicates spectra saturation because of the large amounts of Si−O bonds in the materials. On the other hand, the peaks at 968 and 1639 cm^{-1} represent the groups of Si−OH or H_2O.[30] The peaks of Ti−MCM-41 were very similar to those of MCM-41 except that slight shifts of peaks from 800, 968, and 1639 cm^{-1} toward lower energy are observed. There has been no direct evidence for the shifts of 800 and 1639 cm^{-1} to lower energy as searched from literature data. However, it was observed in the literature[31] that if Si−OH groups were replaced by Ti ligands, the peak at ca. 968 cm^{-1} would gradually disappear while another peak appeared at a lower band of ca. 943 cm^{-1} due to the formation of Ti−O−Si bridges.

To further explore the state of the titanium species, the Ti−MCM-41 samples were subjected to X-ray photoelectron spectroscopic (XPS) analysis and the results are shown in Figure 5. The Ti $2P_{3/2}$ regions show two doublets peaks for the Ti−MCM-41. As seen from the curve-fitted spectra, according

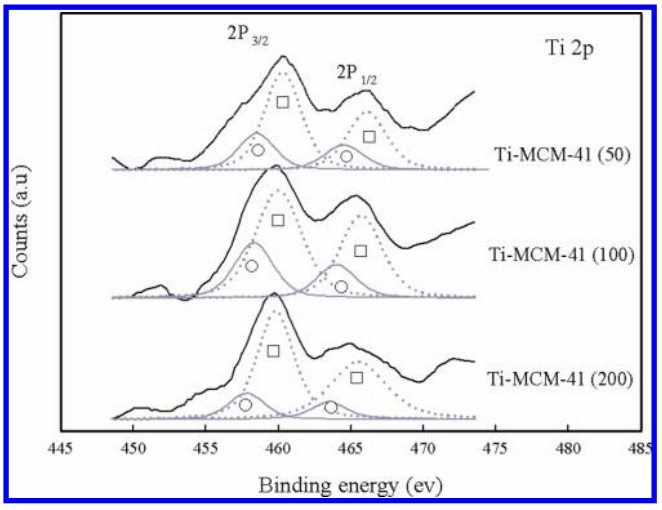

Figure 5. XPS spectra of Ti−MCM-41.

dx.doi.org/10.1021/ie403742j | Ind. Eng. Chem. Res. 2014, 53, 11221−11227

to the literature,[32−34] these may correspond to titanium in tetrahedral (higher binding energy (BE), square symbols) and octahedral coordinated Ti (lower BE, circle symbols).[35,36] The octahedral coordination may be derived from the conversion of tetracoordinated titanium located at the surface of the material to octahedrally coordinated titanium by reaction with $H_2O(g)$ in the atmosphere as well as to segregation of TiO_2 species at the surface of the materials.[32] However, the XPS might still have not provided sufficient evidence on the difference between tetrahedral and octahedral Ti^{4+} sites; further studies using X-ray absorption near edge structure (XANES) or electron paramagnetic resonance (EPR) may be encouraged to clarify this.

Figure 6 shows the UV−vis absorption spectra obtained by diffuse reflection of MCM-41 and Ti−MCM-41. The

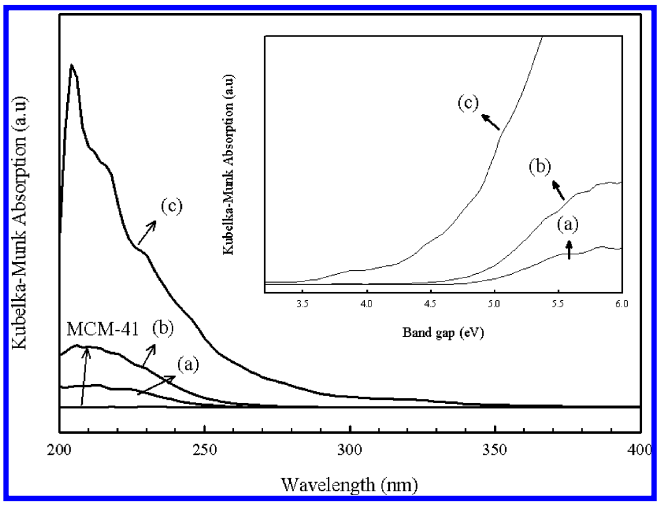

Figure 6. UV−vis absorption spectra obtained by diffuse reflection of (a) Ti−MCM-41(200), (b) Ti−MCM-41(100), and (c) Ti−MCM-41(50).

absorption band spectra were used for the determination of the band gap using the equation of $E_g = 1240/\lambda$ (where λ is wavelength edge of absorption band). For pure MCM-41, no significant UV absorption was observed. For Ti−MCM-41 of different Si/Ti molar ratios, it can be observed that, as the Ti content was increased, the absorption edge was shifted appreciably to longer wavelength. The corresponding band gaps were about 4.85 and 4.5 eV, respectively, for Ti−MCM-41(200) and Ti−MCM-41(50). The absorption of light could be used to further reveal the state of Ti. The absorption in the range between 200 and 230 nm was an electron transport phenomenon;[37−40] i.e., the electrons of O atoms transited to adjacent Ti atoms ($O^{2-} \rightarrow Ti^{4+}$). Thus, the results of FT-IR, UV−vis, and XPS indicated that most of the Ti atoms were tetrahedral Ti^{4+} existing in all materials of Ti−MCM-41. It was also observed for Ti−MCM-41(50) that it had a slight absorption ability after the wavelength of 300 nm. This might be due to the partial aggregation of Ti^{4+} as the Ti content was increased in the structure of Ti−MCM-41.[41]

3.2. Photocatalytic Reduction of CO_2. During the tests, CH_4 and CO are found to be the two detectable reaction products for the CO_2 reduction reaction. Because there might be a carbon source for the reaction other than from CO_2, for example, the MEA reducing agent itself could be the carbon source which led to CH_4 and CO yields, blank tests were performed to clarify this. The results of CH_4 and CO yields with and without blank tests after 8 h of CO_2 reduction reaction are listed in Table 2. Two blank tests were conducted: one without the presence of CO_2 (but with photocatalysts and 0.2 M MEA) and another without the presence of MEA (but with photocatalysts and CO_2). The blank tests without the presence of CO_2 were used to evaluate the contribution of CH_4 and CO yields from MEA, and the results showed that 0.2 M MEA accounted for about 6.2−6.4% of the total CH_4 yield and no CO was formed. On the other hand, the blank tests without the presence of MEA were for understanding the effect of using DI water as the sole solution for the photocatalytic test. When MEA was not present in the solution, CO_2 in the DI water contributed about 7.4−7.7% of the total CH_4 yields and 10.4−15.3% of the CO yields. The effect of direct photoreduction of MEA (without the presence of any photocatalyst and CO_2, but with MEA and UV light source) was also evaluated, where the CH_4 and CO yields were negligible; hence the data are not listed in Table 2. In the following results, all CH_4 and CO yield data with 0.2 M MEA as the reducing agent were presented by subtracting the blank test results from the original total CH_4 and CO yields. Because CH_4 is the main product, the subsequent discussions will focus on the main product of CH_4.

Because NaOH and water are the most commonly used reagents in the literature for the CO_2 photocatalytic reduction,[8,42−45] they were tested and compared with the result using MEA as the absorbent/reductant. The comparison results are shown in Figure 7. The methane production rate with NaOH solution, 1.96 μmol/g of cat., appears to be the lowest among the three solutions. This may be because when NaOH is reacted with high concentration of CO_2, it might

Table 2. Product Yield with and without Blank Tests after 8 h of CO_2 Reduction Reaction

	CH_4 yield (μmol/g of cat.)			
		blank tests		
catalyst	total (with blank)	without CO_2	without MEA	final (without blank)
Ti−MCM-41(100)	69.13 (100.0%)	4.45 (6.4%)[a]	5.13 (7.4%)[a]	59.55 (86.2%)[a]
Ti−MCM-41(50)	72.54 (100.0%)	4.50 (6.2%)	5.62 (7.7%)	62.42 (86.1%)
	CO yield (μmol/g of cat.)			
		blank tests		
catalyst	total (with blank)	without CO_2	without MEA	final (without blank)
Ti−MCM-41(100)	20.02 (100.0%)	N.D.[b] (0.0%)[a]	3.06 (15.3%)[a]	16.96 (84.7%)[a]
Ti−MCM-41(50)	30.84 (100.0%)	N.D.[b] (0.0%)	3.20 (10.4%)	27.65 (89.6%)

[a]The percentages shown in parentheses are the percentages of the total CH_4 and CO yields. The final data shown in the following figures are the total CH_4 and CO yields subtracted from the blank test data. [b]N.D. means the products not detected from GC-FID.

dx.doi.org/10.1021/ie403742j | Ind. Eng. Chem. Res. 2014, 53, 11221−11227

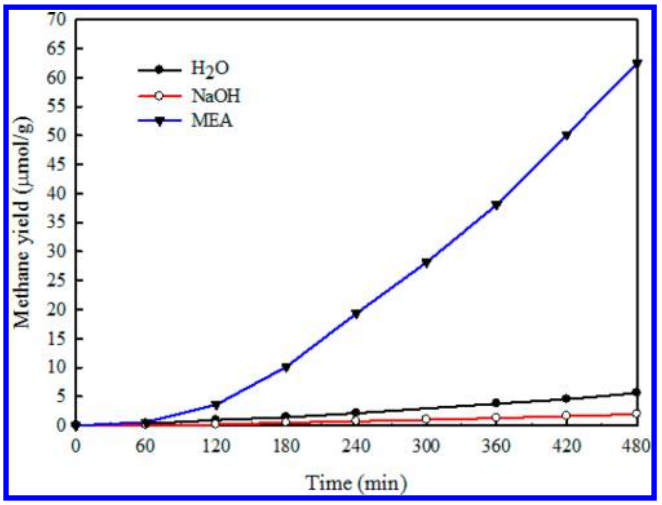

Figure 7. Comparison of methane yields in solutions of MEA, NaOH, and water, respectively, with Ti−MCM-41(50) for the CO_2 photocatalytic reduction reaction.

result in the formation of sodium bicarbonate ($NaHCO_3$) particles and be precipitated in the solution. Thus, the CO_2 concentration could be decreased due to the particle formation and precipitation effects. When MEA was used as the CO_2 absorbent and reductant, the methane yield was greatly enhanced. After 8 h of UV illumination, the methane production rate was 62.42 μmol/g of cat. using MEA, which was about 10 times higher than that of using DI water only: 5.62 μmol/g of cat. This result indicates that CO_2 capture with MEA from flue gas streams and the simultaneous CO_2 utilization to form a CH_4 usable energy source could possibly be integrated into one process.

The photocatalytic activity of Ti−MCM-41 materials was also compared to that of commercial TiO_2 (P25), and the results are shown in Figure 8. After an 8 h test, the results showed that all three Ti−MCM-41 samples had much higher activity than that of TiO_2. This may be because the mesoporous silica materials had higher tendencies for absorbing amines and resulted in more basic surface sites, which was helpful for the reaction with acidic CO_2 molecules.[46] It was also observed from

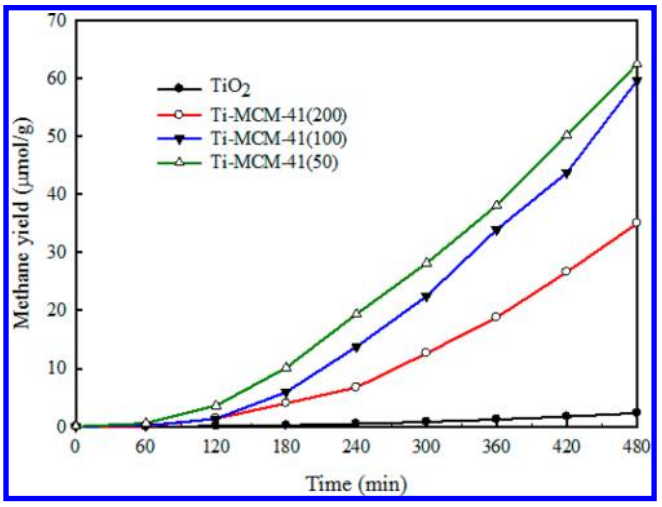

Figure 8. Effect of Si/Ti molar ratios of Ti−MCM-41photocatalysts on the methane yield of CO_2 photocatalytic reduction reaction in MEA solution.

Figure 8 that the methane yield followed the order Ti−MCM-41(50) > Ti−MCM-41(100) > Ti−MCM-41(200). The best methane yield of Ti−MCM-41(50) was because it had the highest Ti metal content of 0.8 wt % while still retaining its high specific surface area of 843 m^2/g as shown in Table 1.

The photocatalytic reduction efficiency of photocatalysts was evaluated in terms of the photoreduction quantum efficiency (PQE) defined by the following equation:[8,43]

$$\mathrm{PQE} = \frac{n_e[\text{mol production yield rate } (\mu\text{mol/h})]}{\text{mol incident UV photon abs rate by cat. } (\mu\text{mol/h})} \cdot 100\% \quad (1)$$

where n_e is the number of moles of electrons required to produce 1 mol of product from reactant. The moles of incident UV photons absorbed by photocatalysts was calculated by the following equation.

$$\text{mol incident UV photons abs by cat.} = \frac{I_{int}\ (\mathrm{W/cm^2})\ A_{proj}\ (\mathrm{cm^2})}{hc/\lambda\ (\mathrm{J/no.\ of\ photons})} \quad (2)$$

where I_{int} is the incident light intensity (32 $\mu W/cm^2$), A_{proj} is the area of light irradiation projected in the reactor (278 cm^2), h is the Planck constant, c is the speed of light, and λ is the wavelength of light (254 nm).

All methane yields of photocatalysts were compared after 8 h of UV illumination, and the total PQEs are summarized in Table 3. The best photoreduction efficiency of photocatalyst

Table 3. Photoreduction Quantum Efficiency (PQE) of Catalysts after 8 h UV Illumination

reducing agent	catalyst	CH_4 yield (μmol/g of cat.)	PQE (%)
H_2O	Ti−MCM-41(50)	5.62	0.83
NaOH	Ti−MCM-41(50)	1.96	0.29
MEA	TiO_2 (P25)	2.32	0.34
	Ti−MCM-41(200)	28.80	5.15
	Ti−MCM-41(100)	59.55	8.76
	Ti−MCM-41(50)	62.42	9.18

was achieved at 9.18% when using the Ti−MCM-41(50) as the photocatalyst and MEA as the absorbent/reductant. This implies that an appropriate amount of Ti content could enhance catalytic activity in the CO_2 reduction reaction.

4. CONCLUSIONS

The photocatalytic reduction of CO_2 with MEA to form methane was studied and compared to those using NaOH and H_2O as the CO_2 reductants. The results indicated that this novel method opens the possibility of integrating the most mature CO_2 capture process of MEA absorption and the CO_2 photocatalytic reduction process into one process. This not only reduces the necessity of storage of CO_2 in the deep sea or underground, but also produces methane as a useful energy source. The experimental results demonstrated that Ti−MCM-41 materials displayed better reaction performance than commercial TiO_2. The Ti−MCM-41(50) could achieve a methane production rate of 62.42 μmol/g of cat. and photoreduction quantum efficiency of 9.18% under UV light. However, the CO_2 reduction tests conducted in this study were at deep UV light (254 nm); this would limit the application of

dx.doi.org/10.1021/ie403742j | Ind. Eng. Chem. Res. 2014, 53, 11221−11227

this process. Thus, future studies should be directed toward the development of photocatalysts which are functional under visible light and also toward the further improvement of photoreduction quantum efficiency.

AUTHOR INFORMATION

Corresponding Author

*Tel.: +886-3-5731868. Fax: +886-3-5725958. E-mail: hlbai@mail.nctu.edu.tw.

Notes

The authors declare no competing financial interest.

ACKNOWLEDGMENTS

Support from the National Science Council, Taiwan, through Grant NSC 99-2221-E- 009-037-MY3 is gratefully acknowledged.

REFERENCES

(1) Pellegrini, G.; Strube, R.; Manfrida, G. Comparative Study of Chemical Absorbents in Postcombustion CO_2 Capture. *Energy* **2010**, *35*, 851.

(2) Strube, R.; Pellegrini, G.; Manfrida, G. The Environmental Impact of Post-Combustion CO_2 Capture with MEA, with Aqueous Ammonia, and with an Aqueous Ammonia-Ethanol Mixture for a Coal-Fired Power Plant. *Energy* **2011**, *36*, 3763.

(3) Yeh, A. C.; Bai, H. Comparison of Ammonia and Monoethanolamine Solvents to Reduce CO_2 Greenhouse Gas Emissions. *Sci. Total Environ.* **1999**, *228*, 121.

(4) Artanto, Y.; Jansen, J.; Pearson, P.; Do, T.; Cottrell, A.; Meuleman, E.; Feron, P. Performance of MEA and Amine-Blends in the CSIRO PCC Pilot Plant at Loy Yang Power in Australia. *Fuel* **2012**, *101*, 264.

(5) Rochelle, G. T. Amine Scrubbing for CO_2 Capture. *Science* **2009**, *325*, 1652.

(6) Stafford, N. Future Crops: The Other Greenhouse Effect. *Nature* **2007**, *448*, 526.

(7) Guo, J.; Zhang, W.; Zhang, M.; Zhang, L.; Bian, X. Will Elevated CO_2 Enhance Mineral Bioavailability in Wetland Ecosystems? Evidence from a Rice Ecosystem. *Plant Soil* **2012**, *355*, 251.

(8) Lee, W.-H.; Liao, C.-H.; Tsai, M.-F.; Huang, C.-W.; Wu, J. C. S. A Novel Twin Reactor for CO_2 Photoreduction to Mimic Artificial Photosynthesis. *Appl. Catal., B: Environ.* **2013**, *132*−*133*, 445.

(9) He, H.; Liu, C.; Dubois, K. D.; Jin, T.; Louis, M. E.; Li, G. Enhanced Charge Separation in Nanostructured TiO_2 Materials for Photocatalytic and Photovoltaic Applications. *Ind. Eng. Chem. Res.* **2012**, *51*, 11841.

(10) Usubharatana, P.; McMartin, D.; Veawab, A.; Tontiwachwuthikul, P. Photocatalytic Process for CO_2 Emission Reduction from Industrial Flue Gas Streams. *Ind. Eng. Chem. Res.* **2006**, *45*, 2558.

(11) Lo, C.-C.; Hung, C.-H.; Yuan, C.-S.; Wu, J.-F. Photoreduction of Carbon Dioxide with H_2 and H_2O over TiO_2 and ZrO_2 in a Circulated Photocatalytic Reactor. *Sol. Energy Mater. Sol. Cells* **2007**, *91*, 1765.

(12) Teramura, K.; Okuoka, S.; Tsuneoka, H.; Shishido, T.; Tanaka, T. Photocatalytic Reduction of CO_2 Using H_2 as Reductant over $ATaO_3$ Photocatalysts (A = Li, Na, K). *Appl. Catal., B: Environ.* **2010**, *96*, 565.

(13) Tseng, I.-H.; Chang, W.-C.; Wu, J. C. S. Photoreduction of CO_2 Using Sol−gel Derived Titania and Titania-Supported Copper Catalysts. *Appl. Catal., B: Environ.* **2002**, *37*, 37.

(14) Elías, V. R.; Vaschetto, E. G.; Sapag, K.; Crivello, M. E.; Casuscelli, S. G.; Eimer, G. A. Synthesis and Photocatalytic Activity of Titania-Loaded Transition Metal-Modified MCM-41 Molecular Sieves. *Top. Catal.* **2011**, *54*, 277.

(15) Chen, Y.-W.; Lin, H.-Y. Characteristics of Ti-MCM-41 and Its Catalytic Properties in Oxidation of Benzene. *J. Porous Mater.* **2002**, *9*, 175.

(16) Huang, M.; Xu, C.; Wu, Z.; Huang, Y.; Lin, J.; Wu, J. Photocatalytic Discolorization of Methyl Orange Solution by Pt Modified TiO_2 Loaded on Natural Zeolite. *Dyes Pigm.* **2008**, *77*, 327.

(17) Kitano, M.; Matsuoka, M.; Ueshima, M.; Anpo, M. Recent Developments in Titanium Oxide-Based Photocatalysts. *Appl. Catal., A: Gen.* **2007**, *325*, 1.

(18) Hayek, K.; Kramer, R.; Paál, Z. Metal-Support Boundary Sites in Catalysis. *Appl. Catal., A: Gen.* **1997**, *162*, 1.

(19) Yang, C.; Liu, P.; Ho, Y.; Chiu, C.; Chao, K. Highly Dispersed Metal Nanoparticles in Functionalized SBA-15. *Chem. Mater.* **2003**, *15*, 275.

(20) Mori, K.; Araki, T.; Shironita, S.; Sonoda, J.; Yamashita, H. Supported Pd and PdAu Nanoparticles on Ti-MCM-41 Prepared by a Photo-Assisted Deposition Method as Efficient Catalysts for Direct Synthesis of H_2O_2 from H_2 and O_2. *Catal. Lett.* **2009**, *131*, 337.

(21) Lin, L.-Y.; Bai, H. Aerosol Processing of Low-Cost Mesoporous Silica Spherical Particles from Photonic Industrial Waste Powder for CO_2 Capture. *Chem. Eng. J.* **2012**, *197*, 215.

(22) Lin, L.-Y.; Bai, H. Facile and Surfactant-Free Route to Mesoporous Silica-Based Adsorbents from TFT-LCD Industrial Waste Powder for CO_2 Capture. *Microporous Mesoporous Mater.* **2013**, *170*, 266.

(23) Kresge, C. T.; Leonowicz, M. E.; Roth, W. J.; Vartuli, J. C.; Beck, J. S. Ordered Mesoporous Molecular Sieves Synthesized by a Liquid-Crystal Template Mechanism. *Nature* **1992**, *359*, 710.

(24) Selvam, P.; Bhatia, S. K.; Sonwane, C. G. Recent Advances in Processing and Characterization of Periodic Mesoporous MCM-41 Silicate Molecular Sieves. *Ind. Eng. Chem. Res.* **2001**, *40*, 3237.

(25) Kong, Y.; Jiang, S.-Y.; Wang, J.; Wang, S.; Yan, Q.; Lu, Y. Synthesis and Characterization of Cu−Ti−MCM41. *Microporous Mesoporous Mater.* **2005**, *86*, 191.

(26) Karthik, M.; Lin, L.-Y.; Bai, H. Bifunctional Mesoporous Cu−Al−MCM-41 Materials for the Simultaneous Catalytic Abatement of NOx and VOCs. *Microporous Mesoporous Mater.* **2009**, *117*, 153.

(27) Chen, Y.-W.; Lu, Y.-H. Characteristics of V-MCM-41 and Its Catalytic Properties in Oxidation of Benzene. *Ind. Eng. Chem. Res.* **1999**, *38*, 1893.

(28) Khalil, K. M. S. Cerium Modified MCM-41 Nanocomposite Materials via a Nonhydrothermal Direct Method at Room Temperature. *J. Colloid Interface Sci.* **2007**, *315*, 562.

(29) Eimer, G. A.; Pierella, L. B.; Monti, G. A.; Anunziata, O. A. Synthesis and Characterization of Al-MCM-41 and Al-MCM-48 Mesoporous Materials. *Catal. Lett.* **2002**, *78*, 65.

(30) Selvaraj, M.; Lee, T. G. A Novel Route to Produce Phthalic Anhydride by Oxidation of O-Xylene with Air over Mesoporous V-Mo-MCM-41 Molecular Sieves. *Microporous Mesoporous Mater.* **2005**, *85*, 39.

(31) Zhao, X. .; Lu, G. .; Hu, X. Characterization of the Structural and Surface Properties of Chemically Modified MCM-41 Material. *Microporous Mesoporous Mater.* **2000**, *41*, 37.

(32) Moretti, G.; Salvi, A. M.; Guascito, M. R.; Langerame, F. An XPS Study of Microporous and Mesoporous Titanosilicates. *Surf. Interface Anal.* **2004**, *36*, 1402.

(33) Eimer, G.; Casuscelli, S.; Ghione, G.; Crivello, M.; Herrero, E. Synthesis, Characterization and Selective Oxidation Properties of Ti-Containing Mesoporous Catalysts. *Appl. Catal., A: Gen.* **2006**, *298*, 232.

(34) Contarini, S.; van der Heide, P. A. W.; Prakash, A. M.; Kevan, L. Titanium Coordination in Microporous and Mesoporous Oxide Materials by Monochromated X-Ray Photoelectron Spectroscopy and X-Ray Auger Electron Spectroscopy. *J. Electron Spectrosc. Relat. Phenom.* **2002**, *125*, 25.

(35) Araújo, R. S.; Azevedo, D. C. S.; Rodríguez-Castellón, E.; Jiménez-López, A.; Cavalcante, C. L., Jr. Al and Ti-Containing Mesoporous Molecular Sieves: Synthesis, Characterization and Redox Activity in the Anthracene Oxidation. *J. Mol. Catal. A: Chem.* **2008**, *281*, 154.

(36) Eimer, G. A.; Chanquia, C. M.; Sapag, K.; Herrero, E. R. The Role of Different Parameters of Synthesis in the Final Structure of Ti-

Containing Mesoporous Materials. *Microporous Mesoporous Mater.* **2008**, *116*, 670.
(37) Galacho, C.; Ribeiro Carrott, M. M. L.; Carrott, P. J. M. Structural and Catalytic Properties of Ti−MCM-41 Synthesised at Room Temperature up to High Ti Content. *Microporous Mesoporous Mater.* **2007**, *100*, 312.
(38) Yamashita, H.; Mori, K. Applications of Single-Site Photocatalysts Implanted within the Silica Matrixes of Zeolite and Mesoporous Silica. *Chem. Lett.* **2007**, *36*, 348.
(39) Yamashita, H.; Anpo, M. Local Structures and Photocatalytic Reactivities of the Titanium Oxide and Chromium Oxide Species Incorporated within Micro- and Mesoporous Zeolite Materials: XAFS and Photoluminescence Studies. *Curr. Opin. Solid State Mater. Sci.* **2003**, *7*, 471.
(40) Anpo, M.; Yamashita, H.; Ikeue, K.; Fujii, Y.; Zhang, S. G.; Ichihashi, Y.; Park, D. R.; Suzuki, Y.; Koyano, K.; Tatsumi, T. Photocatalytic Reduction of CO_2 with H_2O on Ti-MCM-41 and Ti-MCM-48 Mesoporous Zeolite Catalysts. *Catal. Today* **1998**, *44*, 327.
(41) Hu, Y.; Wada, N.; Matsuoka, M.; Anpo, M. Photo-Assisted Synthesis of V-MCM-41 Under UV Light Irradiation. *Catal. Lett.* **2004**, *97*, 49.
(42) Kohno, Y.; Hayashi, H.; Takenaka, S.; Tanaka, T.; Funabiki, T.; Yoshida, S. Photo-Enhanced Reduction of Carbon Dioxide with Hydrogen over Rh/TiO_2. *J. Photochem. Photobiol., A* **1999**, *126*, 117.
(43) Tseng, I.-H.; Chang, W.-C.; Wu, J. C. S. Photoreduction of CO_2 Using Sol−gel Derived Titania and Titania-Supported Copper Catalysts. *Appl. Catal., B: Environ.* **2002**, *37*, 37.
(44) Liu, D.; Quek, X. Y.; Cheo, W. N. E.; Lau, R.; Borgna, A.; Yang, Y. MCM-41 Supported Nickel-Based Bimetallic Catalysts with Superior Stability during Carbon Dioxide Reforming of Methane: Effect of Strong Metal−support Interaction. *J. Catal.* **2009**, *266*, 380.
(45) Zhao, Z.; Fan, J.; Xie, M.; Wang, Z. Photo-Catalytic Reduction of Carbon Dioxide with in-Situ Synthesized $CoPc/TiO_2$ under Visible Light Irradiation. *J. Cleaner Prod.* **2009**, *17*, 1025.
(46) Knowles, G. P.; Graham, J. V.; Delaney, S. W.; Chaffee, A. L. Aminopropyl-Functionalized Mesoporous Silicas as CO_2 Adsorbents. *Fuel Process. Technol.* **2005**, *86*, 1435.